Polymer Degradation and Stability 241 (2025) 111541

Contents lists available at ScienceDirect

Polymer Degradation and Stability

journal homepage: www.journals.elsevier.com/polymer-degradation-and-stability

# Impact of mechanical reprocessing on degradation and performance of PA 11 and PA 11–LDPE blends

Johanna Morales [a], Rose Mary Michell [b], Denis Rodrigue [a,*]

[a] Department of Chemical Engineering, Université Laval, Quebec G1V 0A6, Canada
[b] Institut für Physik, Martin-Luther-Universität, Halle-Wittenberg, Saxony-Anhalt, Halle 06099, Germany

ARTICLE INFO

*Keywords:*
Mechanical recycling
PA 11
Mechanical properties
Reprocessing cycles
Rheological properties

ABSTRACT

This study examines the mechanical recycling of a virgin PA 11 and a post-consumer PA 11–low density polyethylene (LDPE) (90/10) blend over ten reprocessing cycles. Fourier transform infrared spectroscopy (FTIR) and proton nuclear magnetic resonance ($^1$H NMR) analyses revealed changes in the intensity and position of specific absorption bands and proton signals, indicating progressive chain scission and molecular rearrangements. A carbonyl band was identified in the virgin PA 11 after reprocessing, a confirmation of thermo-oxidative degradation. Mechanical testing showed gradual reductions in elastic modulus, stress at break, and impact strength, with significant deterioration from the third cycle onward. Rheological analysis revealed consistent decreases in storage modulus ($G'$), loss modulus ($G''$), complex viscosity ($\eta^*$), and changes in damping factor (tan $\delta$), reflecting lower molecular weight and altered viscoelastic behavior. This was further confirmed via Cole–Cole and van Gurp–Palmen plots. In the post-consumer blend, scanning electron microscopy (SEM) showed progressive coalescence of LDPE droplets, contributing to reduced interfacial area and decreased impact resistance. In general, the results showed that virgin PA 11 retains acceptable performance up to three cycles, while the post-consumer blend exhibits faster and more pronounced degradation driven by both chemical and morphological changes particularly due to droplet coalescence and loss of interfacial area.

## 1. Introduction

Mechanical recycling of polymers has gained significant interest as a sustainable approach to plastic waste reduction and circular economy. While the mechanical recycling of synthetic polymers has been extensively studied, [1] the recycling of biopolymers, especially under multiple reprocessing cycles, remains underexplored. Biobased polymers, such as polyamide 11 (PA 11) derived from castor oil, represent a sustainable alternative to conventional synthetic polymers. Despite its renewable origin, PA 11 is not biodegradable, which reinforces the need for effective recycling strategies to prevent its accumulation in the environment.

PA 11 exhibits a tensile modulus of 1600 MPa with a tensile strength of 49 MPa and an elongation at break reaching 40 % [2–5]. Due to its exceptional chemical and thermal resistance (decomposition temperature around 430–455 °C), [6,7] PA 11 is extensively used in aerospace for lightweight and high-performance components, as well as the automotive industry for fuel tanks, brake lines and bearings. Its resistance against fuels and oils makes it ideal for flexible pipes, while its low water absorption ensure safety in food contact packaging [8,9]. Additionally, PA 11 is used in marine applications for its UV and corrosion resistance, in medical devices for its biocompatibility and strength, as well as oil and gas, sports equipment, and wire/cable industries for its good overall performance [8–10]. These specialized uses, coupled with its relatively high cost [11,12], make PA 11 a strong candidate for primary (closed-loop) recycling, especially inside industrial facilities where material wastes are generated.

Although the mechanical recycling of polyamides offers a sustainable solution to reduce biobased polymers waste, it presents challenges as repeated reprocessing can affect the chemical, physical, mechanical, thermal and rheological properties [13,14]. For instance, Nur-A-Tomal et al. [15] investigated the reprocessing of PA12 over four cycles in injection molding, reporting a 6 % decrease in tensile strength (56.0 MPa to 52.6 MPa) and 10 % in impact strength (11.8 kJ/m$^2$ to 10.6 kJ/m$^2$), mainly attributed to molecular weight reduction (chain scission) caused by thermal degradation. Hirsch and Theumer [14] studied the recycling of a biobased composite of PA 11 with 30 wt. % beech wood particles subjected to two injection molding cycles. Their study

* Corresponding author.
*E-mail address:* denis.rodrigue@gch.ulaval.ca (D. Rodrigue).

https://doi.org/10.1016/j.polymdegradstab.2025.111541
Received 10 May 2025; Received in revised form 1 July 2025; Accepted 10 July 2025
Available online 10 July 2025

revealed a 18 % reduction in tensile modulus with a 19 % decrease in tensile strength, highlighting the loss of mechanical property induced by recycling.

This study investigates a real-world case of post-industrial recycling involving a PA 11–LDPE blend recovered from windmill blade packaging waste. While this system is not representative of a large-scale case on commodity-polymer recycling challenges [16,17], it reflects a relevant closed-loop scenario where recycling occurs within the same manufacturing setting. Thus, it provides valuable insight into the degradation behavior of biobased specialty polymers under multiple reprocessing cycles.

The mechanical recycling behavior of virgin PA 11 and its 90/10 blend with LDPE was evaluated over ten reprocessing cycles using twin-screw extrusion. To streamline the analysis, samples were characterized after 1st, 3rd, 5th, 7th and 10th cycles to determine the effects of reprocessing on different properties. Our previous study showed that the thermal properties of virgin and post-consumer PA 11 were relatively stable after 10 reprocessing cycles [18]. In contrast, this work reports clear changes in mechanical, rheological, and morphological properties providing insight into the recyclability of bio-based PA 11 and its blends for industrial reuse.

## 2. Materials and methods

### 2.1. Materials

The virgin PA 11 used was RILSAN® BESNO TL purchased from Arkema (USA) with a density of 1020 kg/m$^3$ and a melt flow index (MFI) of 1 g/10 min (2.16 kg, 235 °C) [19]. The post-consumer PA 11 is a blend of PA 11 with LDPE (90/10) and supplied by MRC La Haute-Gaspésie (Canada) coming from windmill packaging (windmill blades wrapping).

### 2.2. Preparation of recycled material

The post-consumer PA 11 was received as films, then cut and reprocessed in a co-rotating twin-screw extruder (Leistritz ZSE-27, Germany) with a length/diameter (L/D) ratio of 40 and 10 heating zones (die diameter = 2.7 mm). The total flow rate was 0.5 kg/h and the screw speed was set at 70 rpm. Since PA 11 has a melting temperature ($T_m$) around 190 °C, [20] the temperature profile was set as: 175 °C for the first zone (feed), 210 °C for the second zone, 220 °C for the third zone, 235 °C for the fourth to the eighth zone, 225 °C for the ninth zone and 195 °C for the tenth zone (die) to limit degradation. The glass transition temperature ($T_g$) of PA 11 ranges between 45 and 55 °C. Therefore, the extrudates were cooled using tap water at room temperature (20–25 °C). Finally, the filament was pelletized using a Conair model 304 pelletizer (Conair, USA) and then oven dried for 4 h at 80 °C to remove any moisture left.

### 2.3. Reprocessing cycles

The samples were reprocessed in the same co-rotating twin-screw extruder up to 10 times with the same conditions as mentioned above. Samples were taken after the 1st, 3rd, 5th, 7th and 10th reprocessing cycles for analysis. This methodology was used for both the virgin and post-consumer PA 11. Finally, the samples were oven dried for 4 h at 80 °C to eliminate residual moisture. More information can be found in the first part of this study [18].

### 2.4. Characterization

#### 2.4.1. Fourier transform infrared spectroscopy (FTIR)

FTIR was carried out using a Nicolet (USA) Magna-IR 560. The analysis took place at room temperature with a scanning range from 400 to 4000 cm$^{-1}$ and a spectral resolution of 4 cm$^{-1}$ over 64 scans. The carbonyl index (CI) was determined as the ratio of the absorption at 1741 cm$^{-1}$ to the absorption at 720 cm$^{-1}$ which was found to be insensitive to oxidation.

#### 2.4.2. Proton nuclear magnetic resonance ($^1$H NMR)

The spectra were recorded with an Agilent Technologies (USA) Inova NMR spectrometer at a proton frequency of 400 MHz. The samples were first dissolved in $D_2SO_4$ and then poured into 5 mm OD NMR tubes. A total of 8 scans with a 10 s recycle delay were adequate to yield high-quality spectra. Data acquisition was performed by the VnmrJ 3.2 software and processed with the MestreNova 14.3 software.

#### 2.4.3. Scanning electron microscopy (SEM)

An Inspect F50 SEM (FEI, Hillsboro, OR, USA) was used at an accelerating voltage of 10 kV. The samples were sectioned in the transverse direction from injection-molded specimens using a guillotine cutter after immersion in liquid nitrogen for 15 min to ensure cryogenic fracture and minimize deformation. A thin Au/Pd coating was applied to the exposed surfaces to enhance conductivity. ImageJ software was used to measure the diameter of the LDPE dispersed phase in the blends.

#### 2.4.4. Small amplitude oscillatory shear (SAOS)

Samples were prepared by cutting 25 mm diameter discs from injection-molded specimens with a thickness of 3.1 mm using a metal die and a press. Prior to testing, all samples were pre-heated for at least 10 min to ensure thermal equilibrium and consistent conditions for all samples before starting measurements. Small amplitude oscillatory shear (SAOS) measurements were carried out using a strain-controlled ARES G2 rheometer (TA Instruments, USA) under a nitrogen (inert) atmosphere to prevent polymer degradation at high temperatures. The experiments were conducted using a parallel plate geometry (25 mm diameter) with a fixed gap of 2 mm. This configuration was selected to accommodate the high viscosity of the materials and to reduce edge effects and sample overflow at elevated temperatures. To determine the linear viscoelastic regime (LVR), strain sweep tests were first performed at a constant angular frequency ($\omega$ = 1 rad/s) over a strain range of 0.1–100 %. A strain amplitude of 8 % was then selected for subsequent frequency sweeps, conducted in the range of 0.03 to 50 rad/s. All tests were performed at 240 °C for both virgin and post-consumer PA 11.

#### 2.4.5. Tensile properties

The final samples were produced by injection molding on a PN60 (Nissei, Japan) machine. The injection temperature profile was set as 225–225–224–221 °C (nozzle, front, middle and rear, respectively) with a mold temperature at 30 °C and injection pressure of 45 MPa. The mold has four cavities to directly produce the geometries needed: two dumbbell shapes (type IV of ASTM D638) and two rectangular bars (width and thickness of 12.45 × 3.14 mm$^2$ with two lengths of 80 and 125 mm). Tensile testing was carried out at ambient temperature according to ASTM D638 using a 5000 N load cell and a strain rate of 10 mm/min on an Instron (USA) model 5565 universal mechanical tester. At least 10 dog bone specimens (type IV) with a thickness of 3.1 mm were used. The average values for the stress at break, tensile modulus and elongation at break were calculated with their respective standard deviations.

#### 2.4.6. Notched charpy impact strength

The notched Charpy impact strength was determined at room temperature using a Tinius Olsen (USA) model 104 tester according to ASTM D256. Each formulation used a minimum of ten specimens with dimensions of 60 × 12.7 mm$^2$. Prior to testing, the samples were V-notched using a Dynisco (USA) model ASN 120 m sample notcher 24 h before testing.

#### 2.4.7. CIELab measurements

The color of the tensile specimens was measured at room temperature using a X-Rite spectrophotometer from the Ci6X series (model Ci62)

following ASTM D2244–16. The CIELab parameters ($L^*$, $a^*$ and $b^*$) were recorded to quantify color changes associated with thermal oxidation and reprocessing-induced degradation. This approach provides a quantitative assessment of color changes, which are sensitive indicators of oxidation [21,22]. The color difference ($\Delta E^*$) was calculated as:

$$\Delta E^* = \sqrt{(\Delta L^*)^2 + (\Delta a^*)^2 + (\Delta b^*)^2} \quad (1)$$

where $L^*$, $a^*$ and $b^*$ represent the lightness, green–red, and blue–yellow coordinates, respectively. The measurements were performed directly on the surface of injection molded specimens using standard illumination (D65) and a 10° observer angle. Five replicates were taken per sample to ensure reproducibility.

## 3. Results and discussions

### 3.1. Chemical structure analysis

#### 3.1.1. Fourier transform infrared spectroscopy (FTIR)

The FTIR spectra of virgin and post-consumer PA 11 at various reprocessing cycles are presented in Fig. 1, while the main absorption bands, associated with PA 11 functional groups, are listed in Table 1 for reference.

Pliquet et al. [26] noted that the band at 3080 $cm^{-1}$, corresponding to N–H stretching in secondary amides, can be used to follow structural changes related to thermo-oxidative degradation in polyamides. Additionally, thermal degradation is typically associated with the formation of carbonyl groups, which appear in the 1700–1800 $cm^{-1}$ region due to chain scission [27,28]. Virgin PA 11 (Fig. 1a) exhibits the expected bands listed in Table 1 and the 3080 $cm^{-1}$ band remained unchanged across all reprocessing cycles, suggesting that the overall N–H stretching vibration associated with secondary amides is not significantly affected [29]. However, a distinct carbonyl band at 1741 $cm^{-1}$ was consistently observed in all reprocessed samples, from the 1st to the 10th cycle. This peak is indicative of carboxylic acid end groups formed through oxidative chain scission, confirming that chemical degradation progressively occurs during reprocessing [9,30–33]. The calculated CI, based on the area ratio between the 1741 and 720 $cm^{-1}$ bands, increased from 0.076

**Table 1**
FTIR absorption bands and vibrational assignments for PA 11 [23–25].

| IR bands [$cm^{-1}$] | Assignment |
|---|---|
| 3297 | N–H stretching vibration involved in hydrogen bonding, typically associated with the crystalline domains of PA 11 |
| 3079 | N–H stretching in secondary amides, may also involve overtone coupling with amide II and C–N stretching |
| 2918 | Asymmetric stretching of methylene ($CH_2$) groups along the aliphatic backbone |
| 2850 | Symmetric stretching of $CH_2$ groups in the polymer chain |
| 1635 | Amide I band, mainly $C=O$ stretching with contributions from C–N stretching and backbone deformation |
| 1544 | Amide II band, involving N–H bending and C–N stretching vibrations |
| 1277 | Amide III band, typically assigned to C–N stretching and N–H deformation modes |
| 720 | $CH_2$ rocking deformation, typically linked to crystalline packing in aliphatic chains |

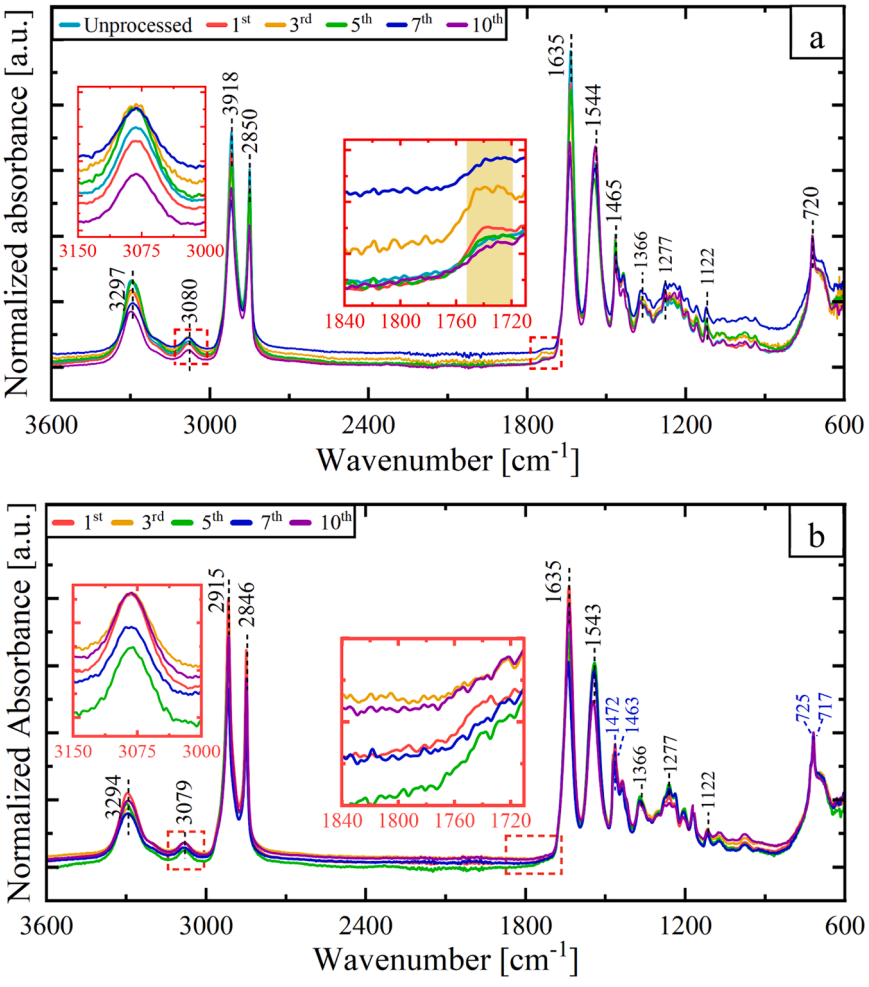


**Fig. 1.** FTIR spectra for: (a) virgin PA 11 and (b) post-consumer PA 11.

in the 1st cycle to a maximum of 0.196 for the 5th cycle, followed by a decrease to 0.057 and 0.088 in the 7th and 10th cycles, respectively. The changes observed across the samples can be associated with progressive degradation [34]. In addition to carbonyl formation, virgin PA 11 presents a localized structural change, as evidenced by the increase in the intensity and a slight shift to higher wavenumbers of the 1544 $cm^{-1}$ band (amide II, N–H bending and C–N stretching). These changes indicate modifications in hydrogen bonding and local chain conformation [35]. This interpretation is further discussed in the $^1$H NMR section.

The post-consumer blend (Fig. 1b) displays additional absorption bands associated with LDPE, especially at 2914 and 2849 $cm^{-1}$ ($CH_2$ stretching), 1472 and 1463 $cm^{-1}$ ($CH_2$ bending), as well as 725 and 719 $cm^{-1}$ ($CH_2$ rocking in the crystalline and amorphous domains, respectively) [25,36]. These bands confirm the presence of LDPE and provide reference to identify changes in the polyolefin phase. For the 3080 $cm^{-1}$ band, it also remained unchanged across all reprocessing cycles, indicating no significant alterations in the global N–H environment. In contrast to virgin PA 11, the carbonyl band at 1741 $cm^{-1}$ was not observed in the post-consumer blend, suggesting that carbonyl groups were not formed in detectable amounts. Similar results were observed for petroleum-based polyamides and LDPE. For example, Su et al. [37] reported no observable changes in the FTIR spectra of PA 6 after 16 mechanical reprocessing cycles performed by injection molding. Similarly, Yap et al. [38] observed no formation of new functional groups in PA 6 after five reprocessing cycles by extrusion. For LDPE, Abad et al. [28] investigated its reprocessing by extrusion and identified two competing mechanisms: chain scission significantly reducing viscosity, and crosslinking which could not be detected by FTIR. Therefore, additional characterization using complementary techniques was conducted as described in the following sections.

### 3.1.2. *Proton nuclear magnetic resonance ($^1$H NMR)*

In order to confirm the presence of new functional groups, $^1$H NMR analysis was performed. Fig. 2 illustrates the identification of protons in the repeat unit's chemical structure, while Fig. 3 presents the $^1$H NMR spectra of virgin PA 11. The spectra can be categorized into two main regions: aliphatic and aromatic. Aliphatic hydrogen resonances appear between 0 and 3 ppm, while aromatic hydrogen resonances are observed around 4–8 ppm [39].

Table 2 presents the chemical shifts ($\delta$) for the proton peaks of all samples. A decrease in the peak intensity corresponding to protons at $\delta =$ 1.25, 1.61, 2.53 and 3.38 ppm, associated with H3–H8, H9/H12, H10 and H1 respectively [40,41], was observed for virgin PA 11. The decreasing trend becomes noticeable from the 3rd cycle, suggesting the presence of multiple degradation mechanisms. Oliviera et al. [27] proposed that the reduction of the peak intensity corresponding to the N-vicinal hydrogen atom (H1) in PA 11 results from a preferential attack on this proton during the early stages of degradation. Similar findings were reported for other aliphatic polyamides. For instance, Karstens and Rossbach [42,43] identified a primary attack on the N-vicinal methylene group during the thermo-oxidative degradation of PA 6/PA 66 blends. Kamerbeek et al. [44,45], Luderwald et al. [46,47] and Bahr et al. [48,49] also highlighted scission at the N-alkylamide bond (leading to lower H1 intensity) as a key degradation mechanism for PA 6, PA 66, and PA 12. In contrast, Montaudo et al. [50,51] and Holland et al. [52] suggested that peptide bond scission (resulting in lower H10 intensity) is the predominant degradation pathway for PA 6 and PA 66. Other studies, including Ohtani et al. [53], Dussel et al. [54], Herrera et al. [55,56] and Ballistreri et al. [57], also emphasized peptide bond degradation

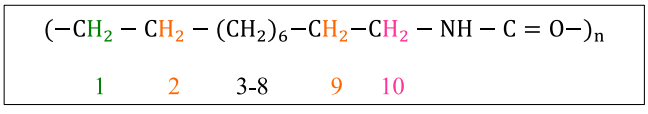


**Fig. 2.** Identification of the protons from the chemical structure of PA 11.

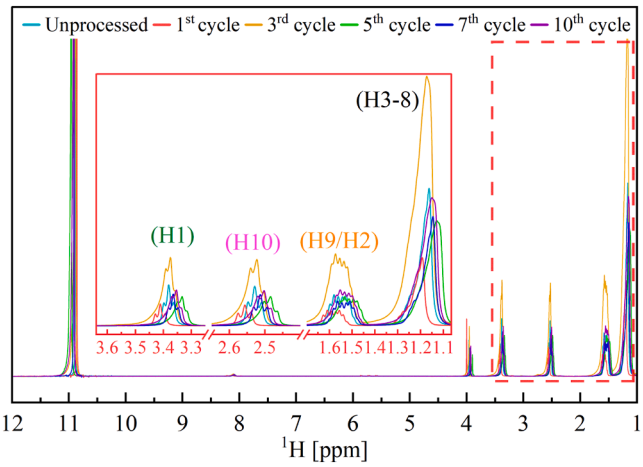


**Fig. 3.** $^1$H NMR spectra of virgin PA 11 for the 1st, 3rd, 5th, 7th and 10th reprocessing cycles.

**Table 2**
Values of δ for the proton peaks of virgin and post-consumer PA 11.

| Sample | Cycle | H1 | H10 | H9/H2 | H3–8 |
|---|---|---|---|---|---|
| Virgin | Unprocessed | 3.38 | 2.53 | 1.61 | 1.25 |
| | 1st | 3.41 | 2.56 | 1.61 | 1.28 |
| | 3rd | 3.37 | 2.52 | 1.56 | 1.18 |
| | 5th | 3.33 | 2.48 | 1.51 | 1.13 |
| | 7th | 3.36 | 2.51 | 1.56 | 1.25 |
| | 10th | 3.35 | 2.50 | 1.53 | 1.21 |
| Post-consumer | 1st | 3.45 | 2.62 | 1.66 | 1.41 |
| | 3rd | 3.46 | 2.61 | 1.65 | 1.41 |
| | 5th | 3.46 | 2.61 | 1.66 | 1.39 |
| | 7th | 3.46 | 2.62 | 1.65 | 1.41 |
| | 10th | 3.45 | 2.61 | 1.65 | 1.38 |

as the primary mechanism. However, they acknowledged that scission at other sites, such as the N-alkylamide bond or the C–C bond (leading to lower H3–8 intensity), can also occur in aliphatic polyamides. These competing mechanisms were corroborated by Hornsby et al. [58] and Levchik et al. [59].

Fig. 4 shows the $^1$H NMR spectra for the post-consumer PA 11. The characteristic LDPE peaks at $\delta = 1.41$ and 1.66 ppm, corresponding to the long chains of aliphatic hydrocarbons[60], are seen in addition to the PA 11 peaks. A slightly lower intensity of the $\delta = 1.41$ ppm peak, attributed to the H3–8 hydrogens in the C–C bonds of the polymer chain,

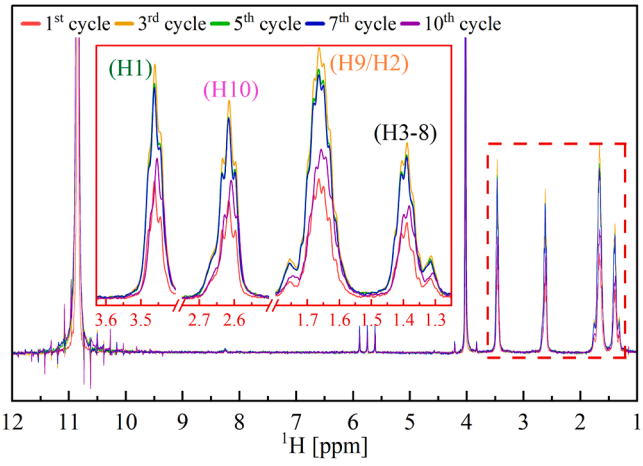


**Fig. 4.** $^1$H NMR spectra for post-consumer PA 11 after the 1st, 3rd, 5th, 7th and 10th reprocessing cycles.

is also observed for post-consumer PA 11. However, no changes were detected at $\delta = 1.66$, 2.62 or 3.45 ppm, corresponding to H9/H12, H10 and H1, respectively. These findings suggest a preferential attack on the H3–8 proton during the degradation for post-consumer PA 11. Finally, distinct peaks are observed in the aromatic region at $\delta = 5.88$, 5.75 and 5.61 ppm. These peaks might be associated with the presence of a yellow pigment in the post-consumer material as discussed later.

### 3.2. Morphological analysis

Morphological analysis was conducted to evaluate the evolution of the LDPE dispersed phase in the post-consumer PA 11 blend and to assess the stability of the initial microstructure throughout reprocessing. Fig. 5 presents SEM images of the post-consumer PA 11 across multiples cycles. At the 1st cycle (Fig. 5a), the LDPE domains are small and uniformly distributed in the polyamide matrix. In the 3rd and 5th cycles (Fig. 5b and c), the domains size increase and exhibit irregular shapes, indicating the presence of both finely dispersed droplets and larger structures. By the 7th and 10th cycles (Fig. 5d and e), fewer domains are observed, and their average size is larger than the other cycles. This morphological evolution indicates coalescence of the dispersed LDPE phase [61].

It is well known that immiscible polymer blends often exhibit distinct phase morphologies and reduced mechanical performance due to poor interfacial adhesion [62–64]. Although PA 11 and LDPE are immiscible because of their polarity contrast, the initial color (yellowish) and microstructure of the blend suggests the presence of compatibilizers or formulation additives promoting interfacial stability and fine dispersion. Such components are frequently added in commercial systems to improve compatibility and enhance mechanical performance [65].

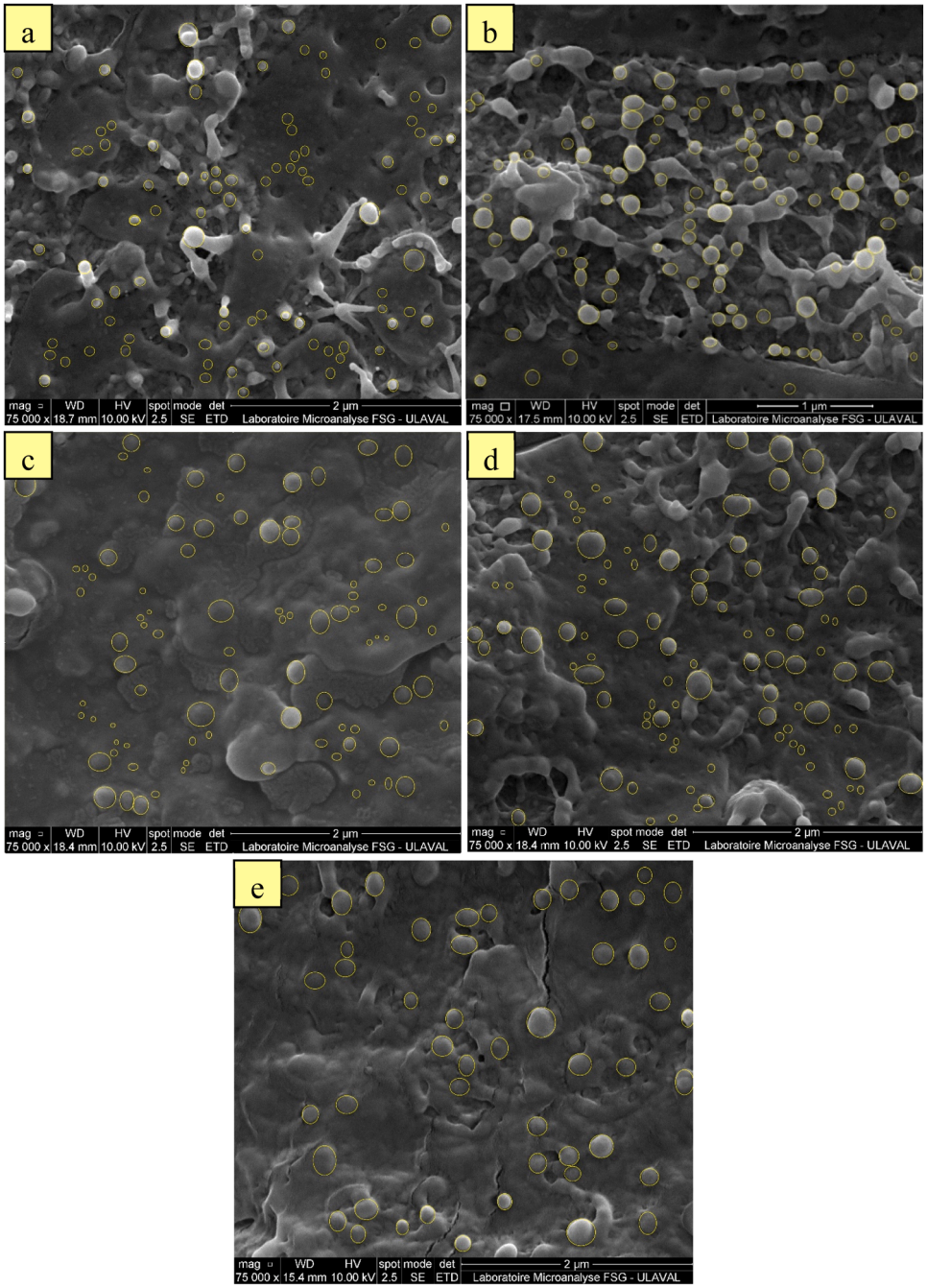


**Fig. 5.** SEM images of post-consumer PA11 over different reprocessing cycles: (a) 1st, (b) 3rd, (c) 5th, (d) 7th and (e) 10th.

During reprocessing, the degradation of these compatibilizers, along with matrix viscosity reduction and lower shear efficiency, likely accelerates droplet coalescence and phase separation [66,67].

To quantify these observations, Fig. 6 presents the particle diameter distribution for each reprocessing cycle. For the 1st cycle, the average diameter is 0.09 μm, with most values between 0.08 and 0.10 μm. For the 3rd and 5th cycles, the distribution becomes bimodal, with the 5th cycle showing a maximum diameter of 0.22 μm and a standard deviation of 0.05 μm. This indicates an unstable morphology with both residual small droplets and growing coalesced domains. For the 7th and 10th cycles, the distribution further shifts to larger values, and the presence of small droplets decreases. The 10th cycle presents the highest average (0.17 μm) with a maximum diameter of 0.25 μm related to the progressive coalescence of LDPE domains with reprocessing.

This coalescence phenomenon, reported in reprocessed blends, reduces the number of interfaces (less droplets) and modifies the phase distribution [61,62]. These morphological changes will influence the mechanical and rheological properties as discussed in the following sections.

### 3.3. Mechanical analysis

#### 3.3.1. Tensile test

Tensile tests were performed to assess the effect of reprocessing on the mechanical performance of virgin and post-consumer PA 11, especially focusing on the tensile modulus, stress at break and elongation at break. These properties are key indicators of polymer recyclability and long-term durability. As shown in Fig. 7, all three tensile properties exhibit a consistent decrease with increasing reprocessing cycles.

For virgin PA 11 (Fig. 7a), the stress–strain curves present a distinct yield point, followed by necking initiation for the unprocessed, 1st and 3rd cycles. This transition is then followed by a second yield point, associated with neck stabilization and propagation [68]. The material subsequently enters a strain hardening region, where multiple stress peaks are observed before the final fracture, which exhibits a fibrillar morphology until the 7th cycle. This post-yield behavior is characteristic of semi-crystalline polyamides with high ductility, indicating effective molecular reorientation and energy dissipation during deformation [69]. The same trend is observed from the 5th cycle to the 10th cycle. However, the strain hardening region becomes less pronounced and fracture occurs sooner after the second yield, revealing a progressive reduction in the material's plastic deformation capacity due to thermo-mechanical degradation [9]. These observations are consistent with the values presented in Fig. 7c showing reductions of 23 % in tensile modulus (643 to 495 MPa), 22 % in stress at break (40 to 31 MPa) and 34 % in elongation at break (268 % to 178 %) between the unprocessed and 10th cycle. These changes are consistent with a reduction in molecular weight (chain scission effect) as previously described for reprocessed polyamides [9,18,37,38,70–79]. Similarly, Ben Amor et al. [70] reported that mechanical reprocessing by injection molding of PA 6 for up to six cycles resulted in a 36 % reduction in Young's modulus and a 14 % decrease in tensile strength. They attributed these losses to molecular weight degradation and impurity accumulation, including thermal degradation byproducts, residues from degraded color masterbatch or environmental particles introduced during grinding and reprocessing. Hirsch and Theumer [14] reported that biobased wood-plastic composites based on PA 11 and beech wood particles showed a 18 % reduction in elastic modulus and a 19 % decrease in tensile strength after two mechanical reprocessing cycles, attributed to thermo-oxidative degradation of both PA 11 and wood particles.

The stress–strain curves of the post-consumer PA 11 (Fig. 7b) present the same general deformation stages as virgin PA 11 (yielding, necking initiation and strain hardening), but with less defined transitions. All samples show a clear yield point followed by necking. After yielding, the stress increases progressively, indicating strain hardening; however, the absence of a distinct stress plateau (as observed in virgin PA 11) suggests modified plastic flow behavior due to the dispersed LDPE phase. Compared to virgin PA 11, the post-consumer blend exhibited lower stress levels, elastic modulus, and yield stress from the first cycle, reflecting the influence of the softer LDPE domains embedded in the polyamide matrix. From the 1st to the 5th cycle, the strain hardening region is present, although the curves exhibit stress fluctuations of lower amplitude followed by a sharper fracture. Since the degree of crystallinity remains relatively constant across cycles, these variations are unlikely to be related to crystalline structure changes. Instead, the reduced elongation at break and the minor stress fluctuations are attributed to limited interfacial adhesion between the PA 11 and LDPE phases, and to localized fibrillar fracture events observed during mechanical testing [80]. In particular, the 7th cycle shows increased elongation accompanied by minor stress fluctuations after yielding. The specimens exhibited a combination of fibrillar and more brittle, glossy fracture regions, suggesting localized changes in deformation mechanisms. These observations indicate that the stress fluctuations are intrinsic to the material behavior, likely associated with phase rearrangements or interfacial weakening due to progressive LDPE droplet coalescence during reprocessing [81]. In contrast, the 10th cycle exhibits a decrease in both ductility and stress magnitude, reflecting progressive degradation of the PA 11–LDPE structure. This qualitative behavior is consistent with the quantitative results (Fig. 7d) showing a decrease of 14 % in elastic modulus (542 to 466 MPa), 70 % in stress at break (27 to 8 MPa) and 43 % in elongation at break (198 % to 113 %) between the 1st and 10th reprocessing cycle. Kuram et al. [75] reported similar trends for PA 6/PC/ABS blends, where the elastic modulus dropped from 1360 MPa in the first cycle to 664 MPa (51 % lower) after three mechanical reprocessing by injection molding. This behavior was attributed to chain scission and changes in interfacial adhesion between

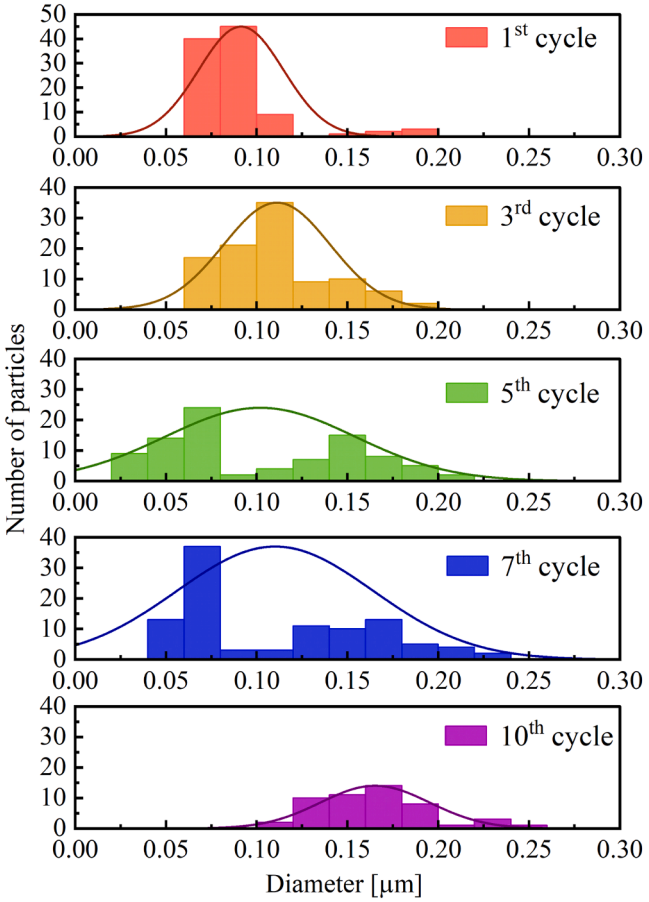


**Fig. 6.** Distribution of diameter of LDPE particles in the post-consumer PA 11.

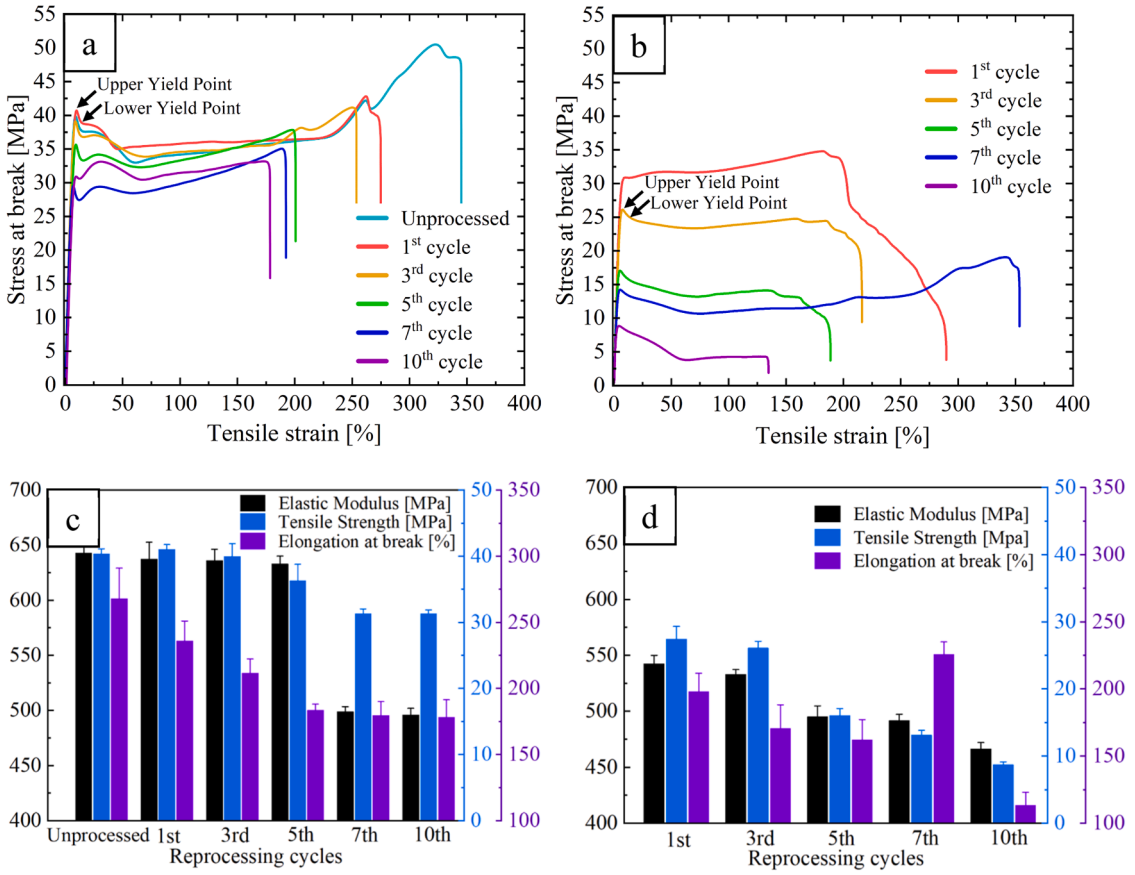


**Fig. 7.** Tensile stress–strain curves for: (a) virgin PA 11 and (b) post-consumer PA 11, and tensile properties (elastic modulus, stress at break and elongation at break) for: (c) virgin PA 11 and (d) post-consumer PA 11 as a function of reprocessing cycles.

the polymer components. In addition, the coalescence of LDPE droplets during reprocessing leads to a reduction in total interfacial area, which further weakens the material by limiting energy dissipation during deformation [62–64].

### 3.3.2. *Impact test*

Fig. 8 presents the notched Charpy impact strength of both virgin and post-consumer PA 11 over different reprocessing cycles. For virgin PA 11, only minor variations are observed. The impact strength slightly increases from 64.9 ± 1.8 J/m for the unprocessed resin to 69.1 ± 1.9 J/m for the 5th cycle, before returning to 63.3 ± 1.6 J/m by the 10th cycle. This relative stability indicates that the virgin polymer maintains sufficient molecular integrity and energy dissipation mechanisms during repeated processing. Nur-A-Tomal et al. [15] observed a similar trend for PA 12, where the impact strength only slightly decreased (10 %) across four injection molding cycles, which was attributed to oxidative and mechanical degradation. Vidakis et al. [82] also found that the mechanical properties of PA 12, including impact strength, initially improved with recycling, but degraded rapidly after the 5th cycle. They associated these changes with structural evolution during reprocessing by extrusion and specific characteristics of the additive manufacturing process.

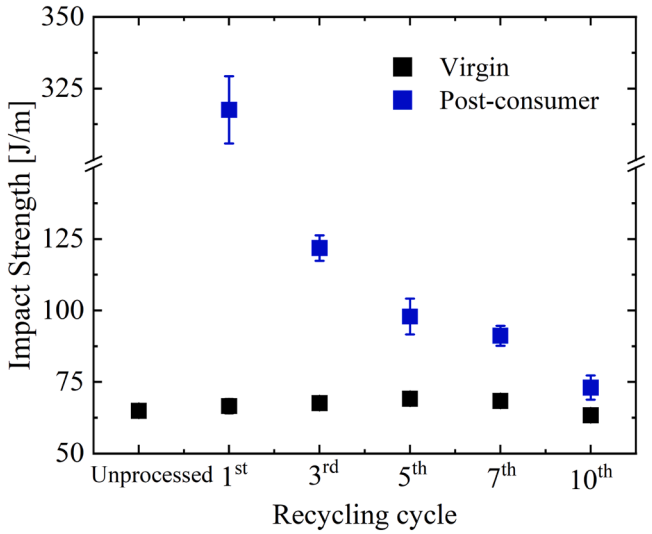


**Fig. 8.** Impact strength of the virgin and post-consumer PA 11.

In contrast, the post-consumer PA 11 showed a significant decrease in impact strength, from 317.5 ± 11.8 J/m in the 1st cycle to 121.8 ± 4.4 J/m in the 3rd cycle and down to 73 ± 4.2 J/m by the 10th cycle. The observed reduction can be attributed to the combined effects of chemical and morphological degradation. While FTIR analyses did not reveal the formation of new functional groups (Fig. 1), $^{1}$H NMR results suggest a preferential attack on the aliphatic backbone (H3–8 region), rather than on the amide bonds, indicating that the degradation mechanism in the post-consumer blend primarily affects the C–C chain segments consistent with chain scission (Fig. 3). Similar degradation mechanisms have been reported by Su et al. [37] during the mechanical recycling of PA6 by injection molding, where the Izod impact strength decreased from 327 J/m to 128 J/m (61 %) after 16 reprocessing cycles. However, the load-extension curves presented in this work showed that the material retained a ductile behavior, with well-defined yield points and extended deformation before failure, even after multiple cycles. In our study, although the impact resistance of post-consumer PA 11 also decreases with reprocessing, it remains higher than that of virgin PA 11,

which may be attributed to the toughening effect of the LDPE phase. This behavior is consistent with classic immiscible blends, where the ductile dispersed phase contributes to energy dissipation and delays brittle fracture. Crespo et al. [76] also reported a significant (36 %) reduction in the Charpy impact strength of PA 6 after five reprocessing cycles by injection molding, associated with the same degradation mechanism.

In addition to chain scission, SEM analysis showed progressive coalescence of the LDPE dispersed phase, especially after the 3rd cycle, leading to fewer and larger domains (Fig. 5, Fig. 6). This reduction in total interfacial area limits energy dissipation during impact, contributing to lower toughness [9,83]. These findings emphasize the role of phase morphology and blend composition in preserving impact resistance during mechanical recycling.

### 3.4. Rheological analysis

#### 3.4.1. Small amplitude oscillatory shear (SAOS)

The frequency-dependent rheological response of virgin and post-consumer PA 11 over different reprocessing cycles was analyzed using SAOS tests as presented in Fig. 9. For virgin PA 11, both the storage modulus ($G'$) and loss modulus ($G''$) exhibited frequency-dependent increases, especially at low frequencies ($\omega < 1$ rad/s) (Fig. 9a,c). The unprocessed sample showed the highest elastic response, with $G'$ exceeding $10^4$ Pa at intermediate frequencies, while the 10th cycle showed values below $10^3$ Pa at $\omega = 0.1$ rad/s and 240 °C. Lee et al. [84] reported similar findings for PA 6, a decrease from above $10^2$ Pa in the unprocessed material at intermediate frequencies to 1 Pa for the 3rd cycle at $\omega = 0.1$ rad/s and 230 °C. They concluded that the differences were related to lower molecular weight. A similar trend was observed for $G''$, suggesting a global reduction in both energy storage and

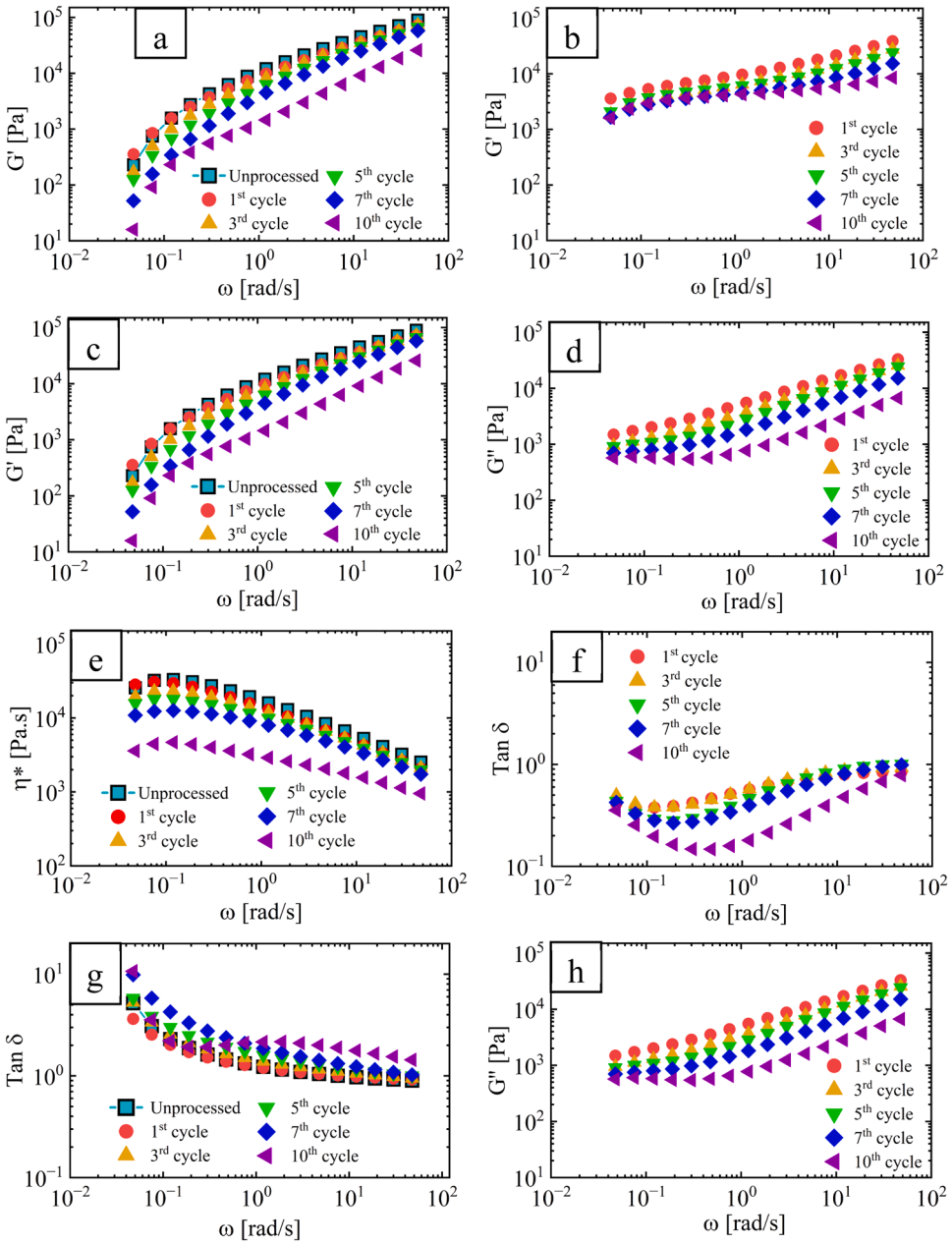


**Fig. 9.** Rheological properties as a function of frequency: (a) storage modulus of the virgin PA 11, (b) storage modulus of the post-consumer PA 11, (c) loss modulus of the virgin PA 11, (d) loss modulus of the post-consumer PA 11, (e) complex viscosity for the virgin PA 11, (f) complex viscosity for the post-consumer PA 11, (g) tan $\delta$ for the virgin PA 11 and (h) tan $\delta$ for the post-consumer PA 11.

dissipation capacities of the melt.

In contrast, the post-consumer PA11 (Fig. 9b, d) shows initially lower $G'$ and $G''$ values, but the moduli decreased more slowly over the cycles. At a frequency of $\omega \approx 0.12$ rad/s, $G'$ decreased from 5328 Pa (1st cycle) to 2948 Pa (10th cycle), a 45 % reduction, while $G''$ decreased from 2011 Pa to 581 Pa, corresponding to a 71 % decrease. In particular, $G'$ remained higher than $G''$ across the entire frequency range, even after 10 cycles, indicating that the material retained a predominantly elastic response. This behavior is associated with the biphasic morphology of the blend. Although the LDPE phase is fully molten at the testing temperature, its presence as a dispersed phase contributes to the viscoelastic profile by influencing the stress distribution and deformation pathways. The progressive reduction in both moduli is consistent with morphological degradation mechanisms, such as droplet coalescence and decreased interfacial adhesion, as observed in Fig. 5 and Fig. 6.

Fig. 9e and f present the evolution of the complex viscosity ($\eta^*$) for the virgin PA11 and the post-consumer blend, respectively. For virgin PA11, $\eta^*$ decreased significantly across all frequencies with successive reprocessing cycles. At a representative frequency of $\omega \approx 0.12$ rad/s, $\eta^*$ dropped from 33.1 kPa·s (unprocessed) to 4.69 kPa·s after the 10th cycle, corresponding to a reduction of 86 %. This significant decrease is indicative of chain scission and reduced molecular weight, which reduce the melt's resistance to flow and enhance the shear-thinning behavior [85,86]. Similar trends were reported by Yap et al. [38], Crespo et al. [76], and Su et al. [37] all of them using injection molding for reprocessing, as well as by Lee et al. [84] using extrusion. These studies consistently observed lower viscosity (or higher melt flow rate) and reduced molecular weight in reprocessed PA 6, which were attributed to chain scission during thermo-mechanical degradation.

For the post-consumer PA 11 (Fig. 9f), a similar degradation trend was observed. The initial $\eta^*$ at $\omega \approx 0.12$ rad/s decreased from 77.0 kPa·s in the 1st cycle to 55.9 kPa·s after the 10th cycle, corresponding to a 27 % reduction. This progressive decrease is likewise attributed to thermo-mechanical chain scission and the associated reduction in molecular weight [9].

The damping factor (tan $\delta$), shown in Fig. 9g and h, provides a measure of the relative contribution of the viscous and elastic responses as this parameter is highly sensitive to changes in molecular structure and interfacial dynamics [87]. For virgin PA11 (Fig. 9g), the material exhibits tan $\delta$ values close to or slightly above 1 at low frequencies ($\omega \approx 0.03$ rad/s), indicating a balanced viscoelastic behavior. However, as frequency increases, tan $\delta$ decreases across all cycles, indicating a transition to elastic-dominated behavior at higher shear rates. With reprocessing, the entire tan $\delta$ curve shifts upward, especially at low frequencies. By the 10th cycle, tan $\delta$ values exceed 2 at $\omega < 0.1$ rad/s, suggesting a significant loss of elastic recovery and a dominance of viscous dissipation. This shift reflects the degradation of molecular weight and entanglement density due to chain scission, leading to fewer long-relaxation-time modes [88].

In contrast, the post-consumer PA 11 (Fig. 9h) shows a distinct behavior. At low frequencies ($\omega \approx 0.03$–$0.1$ rad/s), tan $\delta$ displays a U-shaped profile, with a clear minimum between 0.3 and 1 rad/s that becomes more pronounced with reprocessing. The 1st to 7th cycles exhibits minima around 0.5 rad/s, indicative of predominant elastic behavior at intermediate frequencies. By the 10th cycle, the minimum shifts to higher frequencies and the tan $\delta$ values decrease at low $\omega$, reflecting a loss of viscous contribution relative to elasticity. This behavior suggests that rheological degradation in the blend is driven by polymer chain scission and reduced interfacial effectiveness during flow, potentially due to phase destabilization or compatibilizer degradation during reprocessing [89].

### 3.4.2. Cole–Cole representation

Fig. 10 presents the viscoelastic behavior of virgin and post-consumer PA11–LDPE blends during reprocessing through Cole–Cole plots and phase-space representations of the complex viscosity. In Fig. 10a, the Cole–Cole plot of virgin PA11 shows a quasi-linear relationship between $G'$ and $G''$ for all cycles, with a shift toward lower moduli as the number of reprocessing cycles increases. The unprocessed sample exhibits the highest $G'$ and $G''$ values, indicating a more structured and entangled polymer matrix. As the cycles progress, the data progressively shorten and shift downward, forming a series of diagonal lines of decreasing length. This reduction in curve length is associated with molecular weight degradation, consistent with the observed drop in complex viscosity and moduli in Fig. 7. The contraction of the Cole–Cole arc indicates a decrease in relaxation times and lower elastic

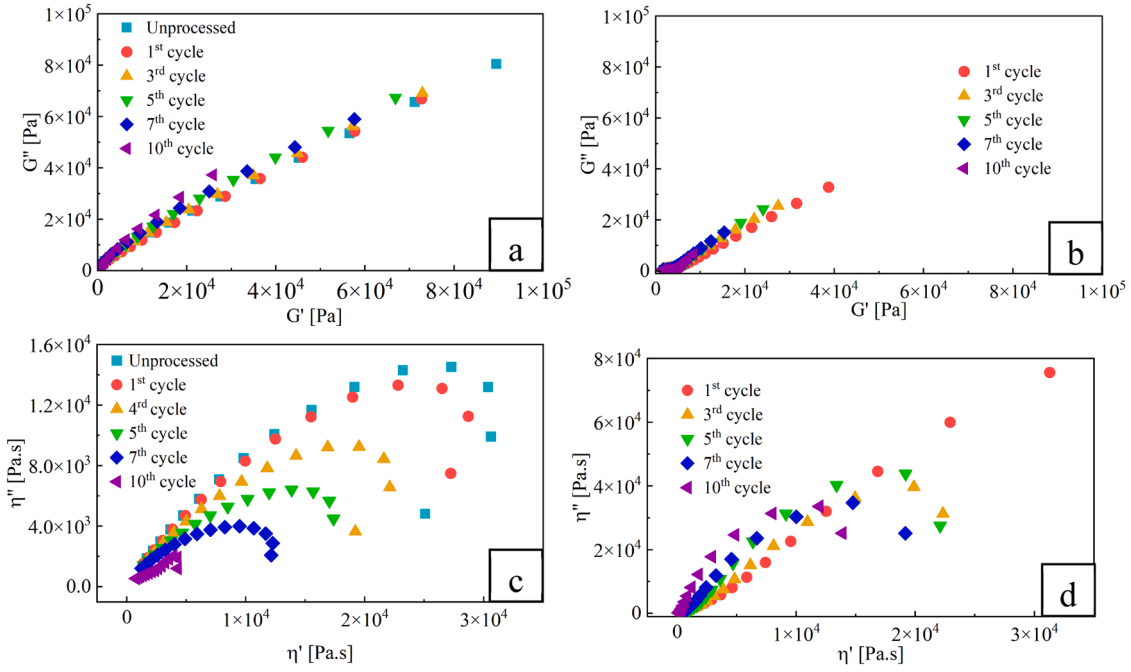


**Fig. 10.** Cole–Cole plots of the systems studied across all reprocessing cycles: $G''$ as a function of $G'$ for: a) virgin PA 11 and (b) post-consumer PA 11 (b); as well as $\eta''$ as a function of $\eta'$ for: c) virgin PA 11 and (d) post-consumer PA 11. All the data were taken at 240 °C.

recovery, suggesting chain scission and reduced entanglement density. A similar trend was reported by Nait-Ali et al. [90] for PET subjected to six reprocessing cycles in an single-screw extruder, where the decrease in curve amplitude was attributed to molecular weight reduction. The absence of curvature or secondary shoulders implies that the polymer remains single-phase, with a continuous distribution of relaxation times [91]. This trend is similar in Fig. 10c, where the plot of $\eta''$ as a function of $\eta'$ shows high viscosity components for the unprocessed and early-cycle samples, while the 10th cycle displays a substantial shift toward lower values, a confirmation a progressive loss of viscoelastic strength due to molecular degradation [92]. A similar observation was reported by Dordinejad et al. [93] who studied the effect of multiple extrusion on LLDPE using a single-screw extruder over 9 reprocessing cycles. In their Cole–Cole plots, the degraded LLDPE samples showed a significant alteration of the $\eta''$–$\eta'$ profile, especially in the high $\eta'$ region. After only three extrusions, the slope of the curve changed from negative to positive, indicating severe structural changes due to thermo-mechanical degradation.

In contrast, Fig. 10b, corresponding to the post-consumer PA11, exhibits a more compact set of Cole–Cole curves, also following a quasi-linear trend. While $G'$ remains higher than $G''$ over all cycles, $G''$ decreases more substantially, especially after the 5th cycle. This reduction is also attributed to the polymer degradation as discussed above. The trend is further supported by Fig. 10d where $\eta''$–$\eta'$ plots for the blend show a narrower spread and a noticeable reduction in $\eta''$ between the 1st and 10th cycles.

In addition, Cole-Cole plots can be used to explore the miscibility characteristics of the blend. In theory, a semi-circular shape in a Cole–Cole viscosity plot is indicative of good miscibility and homogeneous relaxation behavior in polymer blends, as it reflects a broad but continuous distribution of relaxation modes typical of a well-dispersed single-phase system. In contrast, deviations from this shape, such as linear or distorted curves, suggest the presence of multiple phases, inhomogeneous interactions or poor interfacial adhesion [94]. For the post-consumer PA11, the plot shown in Fig. 10d is clearly not semi-circular and follows a quasi-linear trend, even in the early cycles. This linearity confirms that the system is immiscible, with distinct relaxation behavior between the polyamide matrix and the LDPE dispersed phase. These findings are consistent with previous studies on recycled polyamide/polyethylene systems, where linear $\eta''$–$\eta'$ relationships have been used as rheological evidence of heterogeneous phase morphology. For instance, Czarnecka-Komorowska et al. [95] studied a blend composed of 80 wt. % recycled polyethylene and 20 wt. % recycled polyamide 6 and reported a similarly linear Cole–Cole plot related to immiscibility. Even after adding 1 and 3 wt. % of PE-g-MAH as a compatibilizer, the plot remained non-semicircular, highlighting the presence of phase separation in complex recycled blends.

#### 3.4.3. van gurp–palmen representation

In general, van Gurp–Palmen (vGP) plots are used to evaluate and compare the viscoelastic behavior and molecular architecture of polymers. Fig. 11 presents the phase angle ($\delta$) as a function of the magnitude of the complex modulus ($|G^*|$). For virgin PA11 (Fig. 11a), $\delta$ decreases steadily with increasing $|G^*|$, with higher phase angles at low $|G^*|$ indicating a more viscous behavior [96]. As the number of cycles increases, especially by the 10th cycle, the curve shifts upward at low moduli, reflecting a progressive loss of elasticity due to chain scission and reduced entanglement density.

In contrast, the post-consumer blend (Fig. 11b) shows a S-shaped curve with a minimum at $|G^*| < 4$ kPa, indicating a more viscous response at low moduli. However, the 10th cycle exhibits the highest $\delta$ above 4 kPa, reflecting reduced elasticity and a predominance of viscous dissipation at higher stress levels. The overall response remains elastic-dominated, in agreement with the lower tan $\delta$ and Cole–Cole results (Fig. 9, Fig. 10).

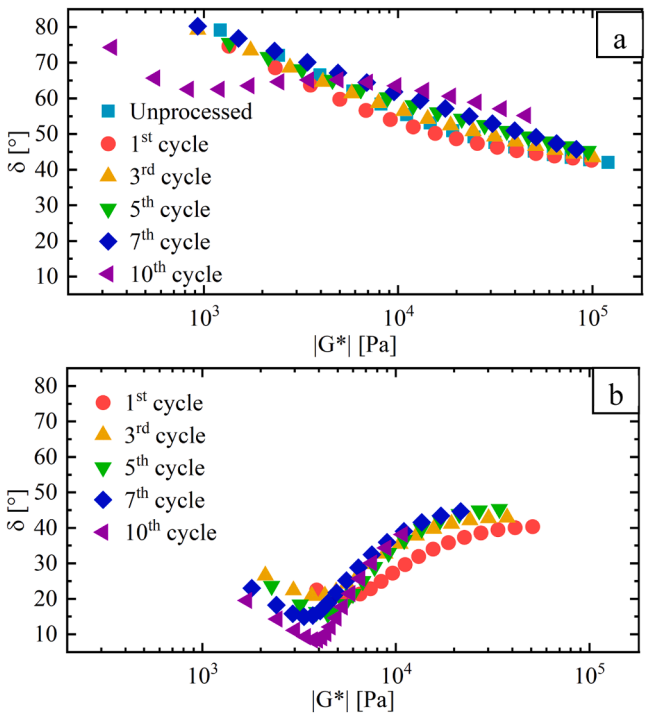


**Fig. 11.** van Gurp–Palmen plots (δ as a function of |G*|) for: (a) virgin PA 11 and (b) post-consumer PA 11 over different reprocessing cycles ($T$ = 240 °C).

### 3.5. Color variation with reprocessing

To evaluate the visual degradation associated with thermo-oxidative processes during reprocessing, colorimetric measurements were conducted using the CIELab color space system. Fig. 12 shows the progressive color change in virgin PA 11 with increasing reprocessing cycles, from its original transparent-white appearance ($L^*$ = 68.9, $a^*$ = 0.1, $b^*$ = –0.1) to a dark brown tone ($L^*$ = 38.9, $a^*$ = 7.6, $b^*$ = 15.0) after 10 cycles. This trend is quantitatively confirmed by the CIELab measurements presented in Table 3. The calculated $\Delta E^*$ values with respect to the unprocessed material show a steady increase with each cycle: 5.3 (1st), 14.2 (3rd), 23.2 (5th), 28.8 (7th), and 33.0 (10th), indicating a strong and visible color shift due to progressive thermo-oxidative degradation [97,98]. In contrast, the post-consumer PA 11 (Fig. 13) starts from a yellowish tone and progress towards a more intense yellow-brown coloration. This is also reflected in the CIELab data, with $\Delta E^*$ values calculated relative to the 1st cycle increasing gradually: 5.8 (3rd), 7.6 (5th), 9.1 (7th), and 12.8 (10th). These discolorations are not only due to thermal degradation, but are also influenced by pigments, stabilizers, and additives present in the original formulation. The color darkening is attributed to the formation of chromophoric structures, such as α,β-unsaturated ketocarbonyls, ketoimides, and pyrrolyl compounds, which originate from radical-induced cleavage of C–N bonds [26,43,99–102]. These species can further react to form oligo-enimine structures, which intensify the visual darkening effect [59,103–105]. The change in color occurs at earlier stages of reprocessing, while mechanical properties remain relatively stable, particularly for virgin PA 11. This suggests that color alterations can serve as an early indicator of material aging before significant structural degradation is detected. However, from a functional perspective, color changes can have limitations on the recyclability of PA 11 in applications where transparency, whiteness, or aesthetic appearance are critical, even if the mechanical performance remains acceptable.

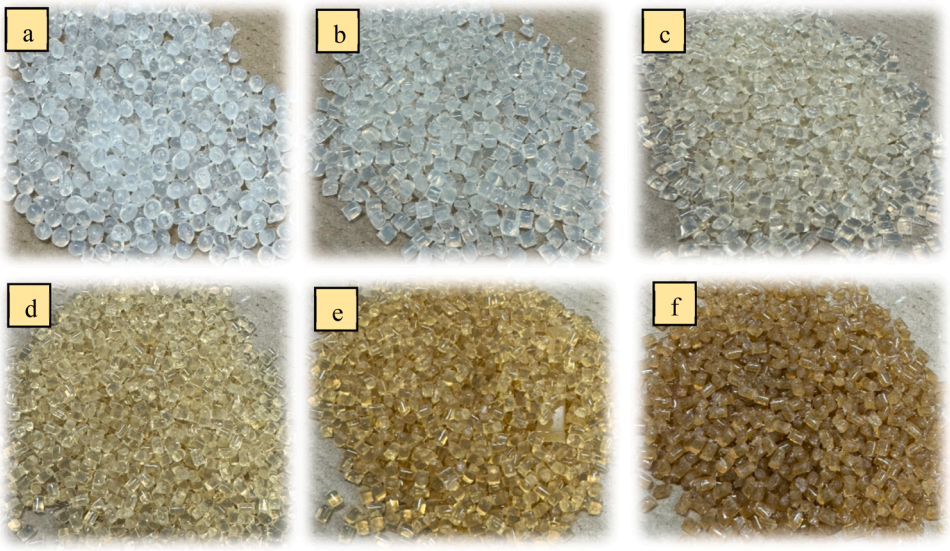


**Fig. 12.** Virgin PA 11 after different reprocessing cycles: (a) virgin, (b) 1st, (c) 3rd, (d) 5th, (e) 7th and (f) 10th.

**Table 3**
CIELab color parameters ($L^*$, $a^*$ and $b^*$) of the virgin and post-consumer PA 11 across reprocessing cycles.

| Sample | Cycle | $L^*$ | $a^*$ | $b^*$ |
|---|---|---|---|---|
| Virgin | Unprocessed | 68.9 ± 0.1 | −0.7 ± 0.1 | 4.0 ± 0.1 |
| | 1st cycle | 66.6 ± 0.6 | −0.7 ± 0.1 | 8.7 ± 0.2 |
| | 3rd cycle | 63.3 ± 0.1 | −0.6 ± 0.8 | 17.0 ± 0.3 |
| | 5th cycle | 58.1 ± 0.1 | 1.3 ± 0.1 | 24.5 ± 0.3 |
| | 7th cycle | 52.1 ± 0.2 | 5.4 ± 0.2 | 26.6 ± 0.4 |
| | 10th cycle | 38.9 ± 0.2 | 7.6 ± 0.2 | 15.0 ± 0.3 |
| Post-consumer | 1st cycle | 58.7 ± 0.1 | −6.1 ± 0.1 | 25.7 ± 1.3 |
| | 3rd cycle | 54.1 ± 0.4 | −4.5 ± 0.1 | 22.4 ± 0.4 |
| | 5th cycle | 53.5 ± 0.2 | −3.2 ± 0.1 | 20.9 ± 0.1 |
| | 7th cycle | 52.2 ± 0.6 | −1.7 ± 0.2 | 20.9 ± 0.8 |
| | 10th cycle | 49.3 ± 0.3 | 0.8 ± 0.1 | 20.5 ± 0.2 |

## 4. Conclusion

This study evaluated the effects of repeated reprocessing (twin-screw extrusion = close-loop mechanical recycling) on the structural, mechanical, morphological and rheological properties of virgin and post-consumer PA 11.

FTIR and $^1$H NMR analyses revealed evidence of molecular degradation during reprocessing, including the appearance of a carbonyl peak at 1741 cm$^{-1}$ in reprocessed virgin PA 11, indicating oxidative chain scission and the formation of carboxylic end groups. Changes in the signals intensity and position associated with specific protons (H1, H10, H3–8) further supported degradation at the N-alkylamide, C–C and potentially peptide bonds. In the post-consumer PA 11–LDPE blend, no carbonyl formation was detected by FTIR, but $^1$H NMR results suggested a preferential attack on the aliphatic backbone (H3–8), consistent with thermo-mechanical degradation.

Mechanically, virgin PA 11 maintained stable performance up to the 3rd reprocessing cycle, with significant reductions observed after the

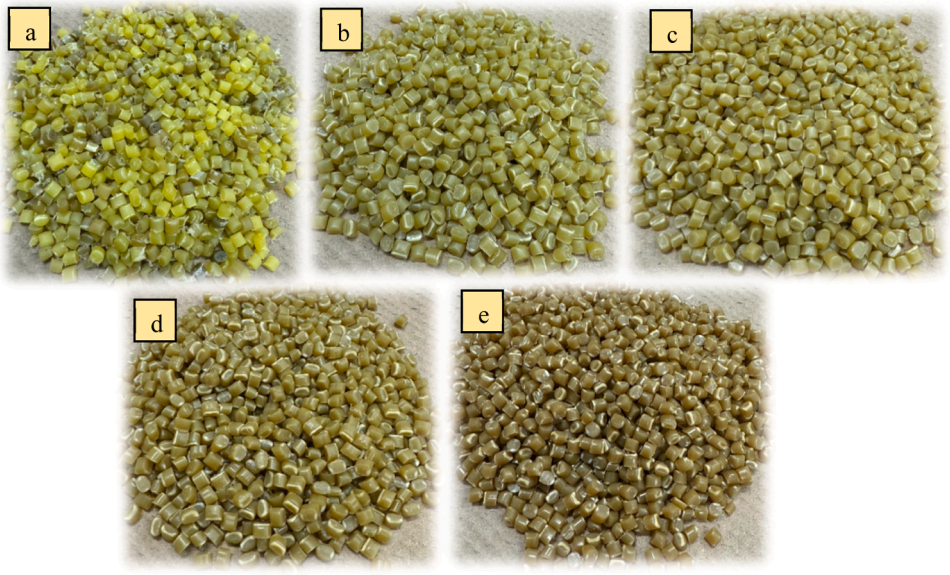


**Fig. 13.** Post-consumer PA 11 after different cycles: (a) 1st, (b) 3rd, (c) 5th, (d) 7th, and (e) 10th cycle.

5th. In contrast, the post-consumer blend showed a sharp decrease in stress at break and impact resistance starting from the 1st cycle. SEM analysis confirmed the progressive coalescence of the LDPE dispersed phase, reducing the total interfacial area and limiting energy dissipation.

Rheological measurements showed consistent decreases in $G'$, $G''$, tan $\delta$ and $\eta^*$, in line with reduced molecular weight and elasticity. Cole–Cole and van Gurp–Palmen plots further revealed structural deterioration and loss of interfacial effects across reprocessing cycles.

Based on the results obtained, the post-consumer PA 11 exhibited faster and more pronounced degradation across mechanical, rheological, and optical analyses, reflecting the combined effects of previous processing history, thermo-oxidative damage, and morphological instability. In contrast, virgin PA 11 maintained better property retention over early cycles before showing significant deterioration at later stages.

Finally, future work should investigate the use of stabilizers, reactive extrusion or compatibilizers to enhance blend stability and extend the recyclability of biobased polymers in circular applications. Additionally, time-dependent rheological experiments (time sweep tests) are recommended to better assess the effect of thermal and structural relaxation effects during reprocessing, especially in polyamide-based systems.

## Ethical approval

This article does not contain any studies with human participants or animals performed by any of the authors.

## CRediT authorship contribution statement

**Johanna Morales:** Writing – original draft, Visualization, Methodology, Investigation, Formal analysis, Data curation, Conceptualization. **Rose Mary Michell:** Writing – review & editing. **Denis Rodrigue:** Writing – review & editing, Supervision, Resources, Project administration, Funding acquisition, Conceptualization.

## Declaration of competing interest

The authors declare that they have no known competing financial interests or personal relationships that could have appeared to influence the work reported in this paper.

## Acknowledgements

The authors acknowledge the MRC La Haute-Gaspésie (Canada) for providing the post-consumer PA 11 material used in this study.

## Data availability

Data will be made available on request.

## References

[1] Z.O.G. Schyns, M.P. Shaver, Mechanical recycling of packaging plastics: a review, Macromol. Rapid Commun. 42 (2021) 2000415, https://doi.org/10.1002/marc.202000415.
[2] M. Niaounakis, Definitions of terms and types of biopolymers, in: M. Niaounakis (Ed.), Biopolymers: Applications and Trends, Biopolymers: Applications and Trends, 1, William Andrew Publishing, Oxford, England, 2015, pp. 1–90. Ch.1.
[3] E. Domingos, et al., Monitoring the polyamide 11 degradation by thermal properties and X-ray fluorescence spectrometry allied to chemometric methods, X-Ray Spectrom. 42 (2013) 79–86, https://doi.org/10.1002/xrs.2436.
[4] Arkema, Arkema celebrates the 70th birthday of its flagship rilsan® polyamide 11 brand, https://www.arkema.com/global/en/media/newslist/news/global/products/technicalpolymers/2017/20170612-Rilsan-anniversar/, 2017, accessed: January 2025.
[5] Xometry, Nylon 11, https://xometry.pro/en/materials/nylon-pa11/, 2024, accessed: January 2025.
[6] N. Sallem-Idrissi, P. Van Velthem, M. Sclavons, Fully bio-sourced nylon 11/raw lignin composites: thermal and mechanical performances, J. Polym. Environ. 26 (2018) 4405–4414, https://doi.org/10.1007/s10924-018-1311-7.
[7] B. Jacques, M. Werth, I. Merdas, F. Thominette, J. Verdu, Hydrolytic ageing of polyamide 11. 1. hydrolysis kinetics in water, Polymer (Guildf) 43 (2002) 6439–6447, https://doi.org/10.1016/S0032-3861(02)00583-9.
[8] W. George, Handbook of Polymers, ChemTec Publishing, Toronto, ON, Canada, 2016.
[9] J. Morales, D. Rodrigue, The effect of reprocessing and moisture on polyamide recycling: a focus on neat, composites, and blends, Macromol. Mater. Eng. (2024) 2400304, https://doi.org/10.1002/mame.202400304.
[10] MatWeb Material Property Data, Isoflon pa 11 polyamide 11, https://www.matweb.com/search/datasheet.aspx?matguid=7b56b1b66c2f4f289d96d263196bdfd7, 2023, accessed: May, 2025.
[11] H. Fiorenza de Lima, M.A. Vaz, M. Ferreira da Costa, A.A. Gomez, G. Lima de Oliveira, Creep behavior of in-service flexible flowline polyamide 11, Polym. Test. 81 (2020) 106205, https://doi.org/10.1016/j.polymertesting.2019.106205.
[12] R. Yu, et al., Preparation and properties of nylon 11/ethylene-vinyl alcohol/montmorillonite ternary composites, Polym. Compos. 41 (2020) 5343–5354.
[13] V. Hirschberg, D. Rodrigue, Recycling of polyamides: processes and conditions, J. Polym. Sci. 61 (2023) 1937–1958, https://doi.org/10.1002/pol.20230154.
[14] P. Hirsch, T. Theumer, Effects of uv aging, water storage and recycling on mechanical properties of biogenic wood-plastic composites from polyamide 11, Macromol. Symp. 403 (2022) 2100509, https://doi.org/10.1002/masy.202100509.
[15] M.S. Nur-A-Tomal, F. Pahlevani, W. Handoko, S.T. Cholake, V. Sahajwalla, Effect of cyclic reprocessing on nylon 12 under injection molding: working toward more efficient recycling of plastic waste, Mater Today Sustain. 11-12 (2021) 100056, https://doi.org/10.1016/j.mtsust.2020.100056.
[16] B. Brehmer, Polyamides from biomass derived monomers, in: S. Kabasci (Ed.), Bio-Based Plastics, Wiley & Sons, Hoboken, NJ, USA, 2013, pp. 275–293. Ch.10.
[17] F.G. de Albuquerque Dias, A.G. Veiga, A.P.A.D.C.P. Gomes, M.L.M. Rocco, M. F. da Costa, Recycling decommissioned polyamide 11: an approach to handle a previously unwanted material, J. Appl. Polym. Sci. 141 (2024) e55195, https://doi.org/10.1002/app.55195.
[18] J. Morales, R.M. Michell, D. Rodrigue, Effect of mechanical recycling on the crystallization of pa 11 and pa 11 ldpe blends, Macromol. Rapid Commun. (2025) 2500164, https://doi.org/10.1002/marc.202500164.
[19] MatWeb Material Property Data, Arkema rilsan® besno tl PA11, https://www.matweb.com/search/DataSheet.aspx?MatGUID=078a73e26ed64ce3bcd70f8695ae222f, 2024, accessed: January 2025.
[20] Campus®, Rilsan® besno tl, https://www.campusplastics.com/campus/en/datasheet/Rilsan%C2%AE+BESNO+TL/ARKEMA/179/5b99ebc9, 2024, accessed: January 2025.
[21] A. Doriat, et al., Assessment of a color measurement-based method for the characterization of polymer thermo-oxidation, Polym. Degrad. Stab. 229 (2024) 110950, https://doi.org/10.1016/j.polymdegradstab.2024.110950.
[22] M. Spencer, et al., Color as a tool for quantitative analysis of heterogeneous polymer degradation, Mater. Today Chem. 29 (2023) 101417, https://doi.org/10.1016/j.mtchem.2023.101417.
[23] D.J. Skrovanek, P.C. Painter, M.M. Coleman, Hydrogen bonding in polymers. 2. infrared temperature studies of nylon 11, Macromolecules 19 (1986) 699–705, https://doi.org/10.1021/ma00157a037.
[24] H.H. Yu, Crystal phase transformations in nylon 11, Macromol. Chem. Phys. 56 (1998) 289–293, https://doi.org/10.1016/S0254-0584(98)00181-3.
[25] V.G. Heidemann, H. Zahn, Beitrag zur deutung des infrarotspektrums von nylon 6, 6, Macromol. Chem. Phys. 62 (1963) 123–133, https://doi.org/10.1002/macp.1963.020620113.
[26] M. Pliquet, M. Rapeaux, F. Delange, P. Bussiere, S. Therias, J. Gardette, Multiscale analysis of the thermal degradation of polyamide 6, 6: correlating chemical structure to mechanical properties, Polym. Degrad. Stab. 185 (2021) 109496, https://doi.org/10.1016/j.polymdegradstab.2021.109496.
[27] M.J. Oliveira, G. Botelho, Degradation of polyamide 11 in rotational moulding, Polym. Degrad. Stab. 93 (2008) 139–146, https://doi.org/10.1016/j.polymdegradstab.2007.10.004.
[28] M.J. Abad, et al., Effects of a mixture of stabilizers on the structure and mechanical properties of polyethylene during reprocessing, J. Appl. Polym. Sci. 92 (2004) 3910–3916, https://doi.org/10.1002/app.20420.
[29] A. Roger, D. Sallet, J. Lemaire, Photochemistry of aliphatic polyamides. 4. mechanisms of photooxidation of polyamides 6, 11, and 12 at long wavelengths, Macromolecules 19 (1986) 579–584, https://doi.org/10.1021/ma00157a015.
[30] P.A. Eriksson, P. Boydell, K. Eriksson, J.A. Månson, A.C. Albertsson, Effect of thermal-oxidative aging on mechanical, chemical, and thermal properties of recycled polyamide 66, J. Appl. Polym. Sci. 65 (1997) 1619–1630, https://doi.org/10.1002/(SICI)1097-4628(19970822)65:8<1619::AID-APP18>3.0.CO;2-Q.
[31] O. Okamba-Diogo, E. Richaud, J. Verdu, F. Fernagut, J. Guilment, B. Fayolle, Molecular and macromolecular structure changes in polyamide 11 during thermal oxidation – kinetic modeling, Polym. Degrad. Stab. 120 (2015) 76–87, https://doi.org/10.1016/j.polymdegradstab.2015.06.005.
[32] S. Maïza, et al., Physicochemical and mechanical degradation of polyamide 11 induced by hydrolysis and thermal aging, J. Appl. Polym. Sci. 136 (2019) 47628, https://doi.org/10.1002/app.47628.
[33] J. Zhang, A. Adams, Understanding thermal aging of non-stabilized and stabilized polyamide 12 using 1H solid-state nmr, Polym. Degrad. Stab. 134 (2016) 169–178, https://doi.org/10.1016/j.polymdegradstab.2016.10.006.

[34] R. Yıldırım, O. Mert, G. Özkoç, M. Kodal, Enhanced recyclability of thermoplastic elastomer toughened polyamide 6 via tri- and multi-epoxy-terminated poss hybrid additives, ACS Omega. 9 (2024) 45467–45486, https://doi.org/10.1021/acsomega.4c07547.

[35] H. Oliver-Ortega, L.A. Granda, F.X. Espinach, M. Delgado-Aguilar, J. Duran, P. Mutjé, Stiffness of bio-based polyamide 11 reinforced with softwood stone ground-wood fibres as an alternative to polypropylene-glass fibre composites, Eur. Polym. J. 84 (2016) 481–489, https://doi.org/10.1016/j.eurpolymj.2016.09.062.

[36] E.R. Ramaswami Sachidanandan, T. Paramanandam, R. Sahadevan, A comparative study on dielectric, structure, and thermal behavior of micro-and nano-sized ccto in nylon 6, 9 matrix, Polym. Compos. 38 (2017) 927–935, https://doi.org/10.1002/pc.23654.

[37] K.-H. Su, J.-H. Lin, C.-C. Lin, Process. technol. influence of reprocessing on the mechanical properties and structure of polyamide 6, J. Mater 192 (2007) 532–538, https://doi.org/10.1016/j.jmatprotec.2007.04.056.

[38] P.P.X. Yap, Z. Yen, T. Salim, H.C.A. Lim, C.K. Chung, Y.M. Lam, The impact of mechanical recycling on the degradation of polyamide, Polym. Degrad. Stab. 225 (2024) 110773, https://doi.org/10.1016/j.polymdegradstab.2024.110773.

[39] Ö.M. Doğan, İ. Kayacan, Pyrolysis of low and high density polyethylene. part II: analysis of liquid products using ftir and nmr spectroscopy, Energ. Sourc. Part A. 30 (2008) 392–400, https://doi.org/10.1080/15567030701457152.

[40] Q.T. Pham, R. Pétiaud, H. Waton, M.F. Llauro-Darricades, in: Q.T. Pham (Ed.), Amides, in Proton & Carbon NMR Spectra of Polymers, Taylor & Francis Group, Boca Raton, 1991, pp. 83–113. Ch.2.

[41] L. Gardella, et al., characterization and stereocomplexation of polyamide 11/polylactide diblock copolymers, Eur. Polym. J.Synthesis (Mass) 98 (2018) 83–93, https://doi.org/10.1016/j.eurpolymj.2017.11.008.

[42] T. Karstens, V. Rossbach, Thermo-oxidative degradation of polyamide 6 and 6,6. kinetics of the formation and inhibition of UV/VIS-active chromophores, Macromol. Chem. Phys. 190 (2003) 3033–3053, https://doi.org/10.1002/macp.1989.021901201.

[43] R. Tian, K. Li, Y. Lin, C. Lu, X. Duan, Characterization techniques of polymer aging: from beginning to end, Chem. Rev. 123 (2023) 3007–3088, https://doi.org/10.1021/acs.chemrev.2c00750.

[44] Kamerbeek, B., Kroes, G., and Grolle, W., "Thermal degradation of some polyamides," in "Khim. Tekhnol. Polim," 1961, vol. 4.

[45] B. Singh, N. Sharma, Mechanistic implications of plastic degradation, Polym. Degrad. Stab. 93 (2008) 561–584, https://doi.org/10.1016/j.polymdegradstab.2007.11.008.

[46] I. Lüderwald, F. Merz, M. Rothe, Über den thermischen abbau des poly-ε-caprolactams (Nylon-6), Macromol. Chem. Phys. 67 (1978) 193–202, https://doi.org/10.1002/apmc.1978.050670114.

[47] C. Alberti, R. Figueira, M. Hofmann, S. Koschke, S. Enthaler, Chemical recycling of end-of-life polyamide 6 via ring closing depolymerization, ChemistrySelect. 4 (2019) 12638–12642, https://doi.org/10.1002/slct.201903970.

[48] U. Bahr, I. Lüderwald, R. Müller, H.R. Schulten, Pyrolysis field desorption mass spectrometry of polymers. III. Aliphatic polyamides, Macromol. Chem. Phys. 120 (1984) 163–175, https://doi.org/10.1002/apmc.1984.051200110.

[49] Z. Zheng, J.L. Yao, Q. Yao, Thermal degradation of polyamide 66 and its model compound, Polym. Degrad. Stab. 228 (2024) 110909, https://doi.org/10.1016/j.polymdegradstab.2024.110909.

[50] G. Montaudo, Mass spectral determination of cyclic oligomer distributions in polymerization and degradation reactions, Macromolecules 24 (1991) 5829–5833, https://doi.org/10.1021/ma00021a017.

[51] C. Wesdemiotis, K.N. Williams-Pavlantos, A.R. Keating, A.S. McGee, C. Bochenek, Mass spectrometry of polymers: a tutorial review, Mass Spectrom. Rev. 43 (2024) 427–476, https://doi.org/10.1002/mas.21844.

[52] B.J. Holland, J.N. Hay, Thermal degradation of nylon polymers, Polym. Int. 49 (2000) 943–948, https://doi.org/10.1002/1097-0126(200009)49:9<943::AID-PI400>3.0.CO;2-5.

[53] H. Ohtani, T. Nagaya, Y. Sugimura, S. Tsuge, Studies on thermal degradation of aliphatic polyamides by pyrolysis-glass capillary chromatography, JAAP 4 (1982) 117–131, https://doi.org/10.1016/0165-2370(82)80003-X.

[54] H.J. Düssel, H. Rosen, D.O. Hummel, Feldionen-und elektronenstoß-massenspektrometrie von Polymeren und Copolymeren, 5. Aliphatische und aromatische polyamide und polyimide, Macromol. Chem. Phys. 177 (1976) 2343–2368, https://doi.org/10.1002/macp.1976.021770811.

[55] M. Herrera, G. Matuschek, A. Kettrup, Main products and kinetics of the thermal degradation of polyamides, Chemosphere 42 (2001) 601–607, https://doi.org/10.1016/S0045-6535(00)00233-2.

[56] J. Guo, C. Luo, Z.K. Chong, A. Alassali, K. Kuchta, Thermal degradation and hydrolysis depolymerization of printing ink components for plastic packaging in recycling processes: a review, Front. Environ. Sci. Eng. 18 (2024) 128, https://doi.org/10.1007/s11783-024-1888-0.

[57] A. Ballistreri, D. Garozzo, M. Giuffrida, G. Impallomeni, G. Montaudo, Primary thermal decomposition processes in aliphatic polyamides, Polym. Degrad. Stab. 23 (1989) 25–41, https://doi.org/10.1016/0141-3910(89)90066-9.

[58] P. Hornsby, J. Wang, R. Rothon, G. Jackson, G. Wilkinson, K. Cossick, Thermal decomposition behaviour of polyamide fire-retardant compositions containing magnesium hydroxide filler, Polym. Degrad. Stab. 51 (1996) 235–249, https://doi.org/10.1016/0141-3910(95)00181-6.

[59] S. Levchik, L. Costa, G. Camino, Effect of the fire-retardant, ammonium polyphosphate, on the thermal decomposition of aliphatic polyamides: part II—Polyamide 6, Polym. Degrad. Stab. 36 (1992) 229–237, https://doi.org/10.1016/0141-3910(92)90060-I.

[60] Q.T. Pham, R. Pétiaud, H. Waton, M.F. Llauro-Darricades, in: Q.T. Pham (Ed.), Olefins, in Proton & Carbon NMR Spectra of Polymers, Taylor & Francis Group, Boca Raton, 1991, pp. 249–293. Ch.7.

[61] A. A.R A.R. Ajitha, S. Thomas, Introduction: polymer blends, thermodynamics, miscibility, phase separation, and compatibilization, in: S. Thomas (Ed.), Compatibilization of Polymer Blends, Elsevier, 2020, pp. 1–29. A. A.RCh.1.

[62] V. Titone, L. Botta, F.P. La Mantia, Mechanical recycling of new and challenging polymer systems: a brief overview, Macromol. Mater. Eng. 310 (2025) 2400275, https://doi.org/10.1002/mame.202400275.

[63] L.A. Utracki, Polyethylenes and their blends, in: L.A. Utracki, C.A. Wilkie (Eds.), Polymer Blends Handbook, Dordrecht, Springer Netherlands, 2014, pp. 1559–1732. Ch.3.

[64] S. Bärwinkel, A. Seidel, S. Hobeika, R. Hufen, M. Mörl, V. Altstädt, Morphology formation in PC/ABS blends during thermal processing and the effect of the viscosity ratio of blend partners, Materials 9 (2016) 659, https://doi.org/10.3390/ma9080659.

[65] M.Y. Khalid, Z.U. Arif, W. Ahmed, H. Arshad, Recent trends in recycling and reusing techniques of different plastic polymers and their composite materials, SM&T 31 (2022) e00382, https://doi.org/10.1016/j.susmat.2021.e00382.

[66] A.D. Patel, Z.O.G. Schyns, T.W. Franklin, M.P. Shaver, Defining quality by quantifying degradation in the mechanical recycling of polyethylene, Nat. Commun. 15 (2024) 8733, https://doi.org/10.1038/s41467-024-52856-8.

[67] J.L. Self, A.J. Zervoudakis, X. Peng, W.R. Lenart, C.W. Macosko, C.J. Ellison, Linear, graft, and beyond: multiblock copolymers as next-generation compatibilizers, JACS Au 2 (2022) 310–321, https://doi.org/10.1021/jacsau.1c00500.

[68] J.W. Hutchinson, K.W. Neale, Neck propagation, J. Mech. Phys. Solids 31 (1983) 405–426, https://doi.org/10.1016/0022-5096(83)90007-8.

[69] O. Frank, J.H. Wendorff, Chain rupture and tensile deformation of polyamide 6 fibers, Colloid. Polym. Sci. 259 (1981) 1047–1055, https://doi.org/10.1007/BF01524889.

[70] I. Ben Amor, O. Klinkova, M. Baklouti, R. Elleuch, I. Tawfiq, Mechanical recycling and its effects on the physical and mechanical properties of polyamides, Polymers 15 (2023) 4561, https://doi.org/10.3390/polym15234561.

[71] D. Matykiewicz, T. Olszewski, J. Andrzejewski, Waste management after the injection process by manufacturing polyamide products based on regranulate, ChemEngineering 7 (2023) 51, https://doi.org/10.3390/chemengineering7030051.

[72] M. Haddar, S. Koubaa, M. Issaoui, A. Frikha, Optimization in the reprocessing of recycled polyamide 6 reinforced with 30 wt % glass fiber (PA6/GF30) using mixture design, Polym. Adv. Technol. 35 (2024) e6240, https://doi.org/10.1002/pat.6240.

[73] M.L. Maspoch, H.E. Ferrando, J.I. Velasco, Characterisation of filled and recycled PA6, Macromol. Symp. 194 (2003) 295–304, https://doi.org/10.1002/masy.200390096.

[74] E. Kuram, E. Tasci, A.I. Altan, M.M. Medar, F. Yilmaz, B. Ozcelik, Investigating the effects of recycling number and injection parameters on the mechanical properties of glass-fibre reinforced nylon 6 using Taguchi method, Mater. Des. 49 (2013) 139–150, https://doi.org/10.1016/j.matdes.2013.02.027.

[75] E. Kuram, B. Ozcelik, F. Yilmaz, The effects of recycling process on thermal, chemical, rheological, and mechanical properties of pc/abs binary and PA6/PC/ABS ternary blends, J. Elastomers Plast. 48 (2015) 164–181, https://doi.org/10.1177/0095244315576.

[76] J.E. Crespo, F. Parres, M.A. Peydró, R. Navarro, Study of rheological, thermal, and mechanical behavior of reprocessed polyamide 6, Polym. Eng. Sci. 53 (2013) 679–688, https://doi.org/10.1002/pen.23307.

[77] M.J. Lozano-González, M.T. Rodriguez-Hernandez, E.A. Gonzalez-De Los Santos, J. Villalpando-Olmos, Physical–mechanical properties and morphological study on nylon-6 recycling by injection molding, J. Appl. Polym. Sci. 76 (2000) 851–858, https://doi.org/10.1002/(SICI)1097-4628(20000509)76:6<851::AID−APP11>3.0.CO;2-D.

[78] M.M. Nir, A. Ram, J. Miltz, Performance of reprocessed multilayer LDPE/nylon-6 film, Polym. Eng. Sci. 35 (1995) 1878–1883, https://doi.org/10.1002/pen.760352307.

[79] R. Scaffaro, L. Botta, M. Mistretta, F.P. La mantia, Processing-morphology-property relationships of polyamide 6/polyethylene blend-clay nanocomposites, Express Polym. Lett. 7 (2013) 873–884, https://doi.org/10.3144/expresspolymlett.2013.84.

[80] M.D.D. Pinzón, C. Saron, Influence of compatibilizer on the properties of low-density polyethylene/polyamide 6 blends obtained by mechanical recycling of multilayer film waste, Waste Manag. Res. 36 (2018) 729–736, https://doi.org/10.1177/0734242×1877779.

[81] Z. Zhang, et al., Surpassing the stiffness-extensibility trade-off of elastomers via mastering the hydrogen-bonding clusters, Matter 5 (2022) 237–252, https://doi.org/10.1016/j.matt.2021.11.007.

[82] N. Vidakis, et al., Sustainable additive manufacturing: mechanical response of polyamide 12 over multiple recycling processes, Materials 14 (2021) 466, https://doi.org/10.3390/ma14020466.

[83] F. Asl, M. Saeb, S.H. Jafari, H.A. Khonakdar, V. Gooadrzi, Conceptualizing physical and chemical interactions in the compatibilized HDPE/PA6 and HDPE/EVOH pairs: theoretical and experimental analyses, Polym-Plast Technol 18 (2017) 1298798, https://doi.org/10.1080/03602559.2017.1298798.

[84] K.H. Lee, S.J. Lim, W.N. Kim, Rheological and thermal properties of polyamide 6 and polyamide 6/glass fiber composite with repeated extrusion, Macromol. Res. 22 (2014) 624–631, https://doi.org/10.1007/s13233-014-2086-x.

[85] R. Salehiyan, S. Soleymani Eil Bakhtiari, A review on rheological approaches as a perfect tool to monitor thermal degradation of biodegradable polymers, KARJ 36 (2024) 295–317, https://doi.org/10.1007/s13367-024-00111-3.
[86] M. Gilbert, Aliphatic polyamides, in: M. Gilbert (Ed.), Brydson's Plastics Materials, Elsevier, Oxford, UK, 2017, pp. 487–511. Ch.18.
[87] Instruments, T.A., Introduction to dynamic mechanical analysis and its application to testing of polymer solids, https://www.tainstruments.com/applications-notes/introduction-to-dynamic-mechanical-analysis-and-its-application-to-testing-of-polymer-solids/, 2025, accessed: April 2025.
[88] W. Thimm, C. Friedrich, M. Marth, An analytical relation between relaxation time spectrum and molecular weight distribution, J. Rheol. 43 (1970) 1663–1672, https://doi.org/10.1122/1.551066.
[89] J. Maris, S. Bourdon, J.-M. Brossard, L. Cauret, L. Fontaine, V. Montembault, Mechanical recycling: compatibilization of mixed thermoplastic wastes, Polym. Degrad. Stab. 147 (2018) 245–266, https://doi.org/10.1016/j.polymdegradstab.2017.11.001.
[90] K.L. Nait-Ali, A. Bergeret, L. Ferry, X. Colin, Chain branching detection by Cole–Cole modeling of rheological properties changes during PET mechanical recycling, Polym. Test. 31 (2012) 500–504, https://doi.org/10.1016/j.polymertesting.2012.01.006.
[91] M.I. Peñas, et al., How is rheology involved in 3D printing of phase-separated PVC-acrylate copolymers obtained by free radical polymerization, Polymers 12 (2020) 2070, https://doi.org/10.3390/polym12092070.
[92] S. Hammani, N. Moulai-Mostefa, P. Samyn, M. Bechelany, A. Dufresne, A. Barhoum, Morphology, rheology and crystallization in relation to the viscosity ratio of polystyrene/polypropylene polymer blends, Materials 13 (2020) 926, https://doi.org/10.3390/ma13040926.
[93] A.K. Dordinejad, F. Sharif, M. Ebrahimi, R. Rashedi, Rheological and thermorheological assessment of polyethylene in multiple extrusion process, Thermochim. Acta 668 (2018) 19–27, https://doi.org/10.1016/j.tca.2018.08.010.
[94] Y. Chen, H. Zou, Y. Cao, M. Liang, Melt miscibility of HDPE/UHMWPE, LDPE/UHMWPE, and LLDPE/UHMWPE blends detected by dynamic rheometer, Polym. Sci. - A. 56 (2014) 630–639, https://doi.org/10.1134/S0965545×14050046.
[95] D. Czarnecka-Komorowska, J. Nowak-Grzebyta, K. Gawdzińska, O. Mysiukiewicz, M. Tomasik, Polyethylene/polyamide blends made of waste with compatibilizer: processing, morphology, rheological and thermo-mechanical behavior, Polymers 13 (2021) 2385, https://doi.org/10.3390/polym13142385.
[96] S. Trinkle, C. Friedrich, Van Gurp-Palmen-plot: a way to characterize polydispersity of linear polymers, Rheol. Acta 40 (2001) 322–328, https://doi.org/10.1007/s003970000137.
[97] G. Pastorelli, et al., Environmentally induced colour change during natural degradation of selected polymers, Polym. Degrad. Stab. 107 (2014) 198–209, https://doi.org/10.1016/j.polymdegradstab.2013.11.007.
[98] R.R.A. Silva, C.S. Marques, T.R. Arruda, S.C. Teixeira, T.V. de Oliveira, Biodegradation of polymers: stages, measurement, standards and prospects, Macromol 3 (2023) 371–399, https://doi.org/10.3390/macromol3020023.
[99] C.H. Do, E.M. Pearce, B.J. Bulkin, H.K. Reimschuessel, Thermal properties of nylons containing carbonyl groups, J. Polym. Sci. Part A Polym. Chem. 24 (1986) 1657–1674, https://doi.org/10.1002/pola.1986.080240723.
[100] L. Sang, C. Wang, Y. Wang, Z. Wei, Thermo-oxidative ageing effect on mechanical properties and morphology of short fibre reinforced polyamide composites–comparison of carbon and glass fibres, RSC Adv. 7 (2017) 43334–43344, https://doi.org/10.1039/C7RA07884F.
[101] B. MAREK, E. LERCH, Photodegradation and yellowing of polyamides, J. Soc. Dyers Colour. 81 (1965) 481–487, https://doi.org/10.1111/j.1478-4408.1965.tb02621.x.
[102] T. Karstens, V. Rossbach, Thermo-oxidative degradation of polyamide 6 and 6,6. kinetics of the formation and inhibition of UV/VIS-active chromophores, Macromol. Chem. Phys. 190 (1989) 3033–3053, https://doi.org/10.1002/macp.1989.021901201.
[103] S. Fan, et al., Yellowing mechanism of PA56 during thermal oxidation process, Polym. Degrad. Stab. 229 (2024) 110970, https://doi.org/10.1016/j.polymdegradstab.2024.110970.
[104] N.S. Allen, J.F. McKellar, G.O. Phillips, Origin and photooxidation of the phosphorescent species in nylon 66, J. Polym. Sci. 13 (1975) 2857–2858, https://doi.org/10.1002/pol.1975.170131221.
[105] P. Ren, et al., Thermal degradation of polyamide 6: mechanisms, mitigation strategies, and challenges, Chem. Eng. Sci. (2025) 121985, https://doi.org/10.1016/j.ces.2025.121985.